



Bael fruit shell–derived activated carbon adsorbent: effect of surface charge of activated carbon and type of pollutants for improved adsorption capacity

Velusamy Mozhiarasi¹ · Thillai Sivakumar Natarajan²

Received: 2 April 2022 / Revised: 29 June 2022 / Accepted: 10 August 2022 / Published online: 24 August 2022
© The Author(s), under exclusive licence to Springer-Verlag GmbH Germany, part of Springer Nature 2022

Abstract

A recyclable activated carbon adsorbent with a highly negative surface charge was synthesized from bael fruit shell waste. The structural, morphological, and surface properties of the activated carbon adsorbent were evaluated using XRD, FE-SEM, FTIR, zeta potential, and BET surface area analysis. The results demonstrated that the surface area of the activated carbon adsorbent got significantly enhanced (944.09 m²/g) as compared to that of the carbonized material (2.43 m²/g) which was validated through FE-SEM analysis. The zeta potential value of activated carbon (− 16.2 mV) reveals that the net surface charge of the activated carbon is negative, which leads to 94.15% removal of methylene blue dye (cationic) as compared to 65.71% and 50.59% removal of rhodamine B (zwitterionic) and reactive red (anionic) dyes, respectively. This could be due to the electrostatic attraction between the cationic methylene blue dye and the negative surface of activated carbon. Furthermore, the adsorption data revealed that 300 mg of activated carbon, 50 ppm initial concentration, and pH of 6.56 are the optimum conditions for enhanced adsorption capacity of activated carbon towards methylene blue pollutant. The adsorption experimental data were best fitted into the Langmuir isotherm and second-order kinetic model ($R^2=0.99–1.00$). In addition, the activated carbon was successfully regenerated and reused up to 5 cycles of adsorption experiments where the adsorption efficiency was retained. Therefore, the bael fruit shell waste–derived activated carbon adsorbent with a high negative surface charge could be a potential alternative to commercial counterparts in the selective removal of pollutants removed from the wastewater stream.

Keywords Bael fruit shell · Activated carbon · Surface charge · Methylene blue

1 Introduction

Large amounts of dye-bearing effluent discharges from various industries like tanneries, textile, paper, cosmetics, and printing are increasing annually due to the increasing rate

of production and consumption [1, 2]. These dyes are usually synthetic in origin and also have a complex aromatic molecular structure that in turn makes them more stable, thereby retarding biodegradation [3]. The annual production of dyes approximates 7×10^5 tons/year whose discharge into the water bodies may cause significant environmental problems due to their high solubility that increases the level of toxicity and chemical oxygen demand, lessen light penetration, etc., into the receiving water streams [4, 5]. This in turn affects aquatic life, crop yield, and health. Some of the commercially used dyes or their degradation products are even carcinogenic and mutagenic [6]. However, these industries discharging dye-bearing effluents play an important role in a country's global export business that supports livelihood. Hence, the removal of the dyes from the industrial effluent discharges is of great importance for well-being.

Several separation techniques are applied in effluent treatment plants for the removal of dyes from effluents

Velusamy Mozhiarasi and Thillai Sivakumar Natarajan equally contributed.

✉ Velusamy Mozhiarasi
mozhiarasi@clri.res.in; mozhi.enviro@gmail.com

✉ Thillai Sivakumar Natarajan
tsknatarajan@gmail.com; thillai@clri.res.in

¹ CLRI Regional Centre, CSIR-Central Leather Research Institute (CSIR-CLRI), Jalandhar 144021, Punjab, India

² Environmental Science Laboratory, CSIR-Central Leather Research Institute (CSIR-CLRI), Chennai 600020, Tamil Nadu, India

like ion exchange, adsorption, precipitation, coagulation, membrane separation, ozonation, and advanced oxidation [7]. However, each technique has its own advantages and disadvantages associated with it. Among various techniques, adsorption for the removal of dyes has gained attention due to its high efficiency, recyclability, environmental benignity, cost-effectiveness, ease of operation, and implementation. Physical adsorption arises when weak forces or bonds like van der Waals, hydrogen, and dipole–dipole exist between the adsorbate and adsorbent. In addition, physical adsorption is reversible in most materials, whereas chemical adsorption arises when strong forces or bonds like covalent or ionic bonds occur between the adsorbate and adsorbent, and it is irreversible [8–10]. Various adsorbents such as nanoparticles, metal oxides, carbon nanotubes, nanotubes, clays, layered materials, silica, industrial solid wastes, activated carbon (AC), and metal–organic frameworks (MOFs) have been developed for adsorptive removal of water pollutants [9, 11–16]. Among these, AC is the widely utilized adsorbent because of its high specific surface area and a high degree of surface reactivity which leads to high adsorption capacity and faster removal rate. However, AC is generally synthesized using commercially available chemical substrates, involves intricate reaction conditions, and is expensive [17, 18].

Recently, agro-residues/biowastes like rice husk, coconut shell, wood char, and almond shell are widely researched to synthesize carbonaceous adsorbents to study their effect on dye removal [19, 20]. There exist several studies on the use of waste-based activated carbon for the removal of dyes. Among various commercial dyes, rhodamine B (RhB) and methylene blue (MB) are widely applied in the making of several products including paper, leather, silk, weed, bamboo, and straw [21, 22]. Both of these dyes can penetrate into the cells easily by reacting with the negatively charged surface of the cell membrane. Methylene blue dyes cause eye burns, dyspnea, methemoglobinemia, skin irritation, and diarrhea if ingested. Likewise, rhodamine B dye also causes eye and skin irritation, gastrointestinal tract irritation, etc. [23]. The adsorption of RhB and MB dyes was carried out using the biochar derived from *Pongamia glabra* seed cover by pyrolysis at 550 °C at a heating rate of 40 °C/min. The optimum biochar demand was found to be 30 g/L for RhB dye and 50 g/L for MB dye with an optimum initial dye concentration of 50 ppm. Malhotra et al. [24] experimented with tea waste–derived carbon for the adsorptive removal of sodium diclofenac at varying concentrations and found the highest adsorption capacity of 62 mg/g by activation of adsorbent using ZnCl_2 . Also, Hou et al. [25] utilized sorghum root and stem as carbon precursors and carried out KOH activation of the resultant char. The adsorptive removal of MB dye was found to be 98%. These findings

reveal the synthesis of sustainable and efficient adsorbents from wastes for the removal of dyes.

Among various feedstocks, the waste shell of the bael fruit (*Aegle marmelos*) is widely available throughout the regions of India and the plant is native to India and Bangladesh. The outer shell of the fruit is hard whereas the inner portion is edible. The fruit is regarded for its multiple medicinal benefits to treat several health disorders like jaundice, obesity, piles, edema, and gynecological and urinary disorders [26, 27]. Apart from the use of inner pulp, the outer shell is a waste, which is mostly discarded along with the municipal solid waste that could be utilized as a feedstock for biochar synthesis to lessen the waste in the dumpsites. An existing study on the use of bael fruit shell waste–based activated carbon for the removal of patent blue dye recorded a dye removal efficiency of 74% with a maximum sorption capacity of 3.7 mg/g (pH of 2.7) in batch adsorption experimentation [28]. In addition, the electrostatic interactions, apart from the π - π interaction, during adsorption rely on the charge and chemical structure of the dye and thus influence the adsorption capacity of ionic pollutants on the adsorbent and also aid selective adsorption [29]. The dispersive interactions are found to be prevalent during the adsorption of dyes on basic activated carbon since the oxygen surface groups of carbon promote the basic dye adsorption. Hence, the charge of the dye is also an influential factor that imparts the adsorption capacity of the dye on the waste-derived carbon. Further, changes in the pH of the initial dye solution could also cause a change in the surface charge of the adsorbent as well as the degree of ionization. For instance, Bhattacharyya et al. [30] observed a low sorption capacity of RhB dye solution using kaolinite (positive surface) under an acidic pH range. However, the applications of the activated carbon from this bael fruit waste shell waste for adsorption of largely available commercial dyes like MB, RhB, and reactive red (RR) were not investigated to the best of our knowledge.

Herein, the current research aim to experiment the performance of bael fruit shell waste (BFSW)–derived activated carbon for the removal of synthetic dyes. Also, the effects of surface charge and type of dyes (cationic, anionic, and zwitterionic) on the adsorption capacity of activated carbon derived from BFSW waste were studied. BFSW was potentially utilized as a feedstock for the synthesis of carbon material. Furthermore, the synthesized carbon was activated using KOH to enhance its physicochemical property for improved pollutant removal. The physicochemical properties of the adsorbent were presented. The adsorption was experimented and analyzed under varying experimental conditions (adsorbent amount, pH, and concentration of pollutants). In addition, the experimental results were fitted in adsorption kinetic and isotherm models.

2 Experimental section

2.1 Materials and methods

Activated carbon (AC) was synthesized from bael fruit shell waste (BFSW). Bael fruit was collected from the campus of the CLRI Regional Centre, Jalandhar, Punjab (Fig. 1a). The shells were removed, cut into small pieces, and dried under sunlight for 2 days (11 a.m – 4 p.m., maximum sunlight intensity) (Fig. 1b). Sodium hydroxide (NaOH, 98.5%), potassium hydroxide (KOH, $\geq 85\%$), hydrochloric acid (HCl, 35–37%), methylene blue (97%), rhodamine B (80%), and reactive red (95%) dyes were purchased from S.D. Fine Chemicals Ltd., Mumbai, India. The molecular structure and chemical properties of dyes are given in Table 1. All the chemicals were used as received, and double-distilled water was used for the preparation of the experimental solution.

2.2 Synthesis of activated carbon

The dried BFSW waste biomass was carbonized in a muffle furnace with temperature control at a heating rate of 10 °C /min to the final temperature of 350 °C and kept at the set temperature for a 2-h reaction time. The resultant carbon was cooled down to room temperature, and the obtained carbon material was rinsed with distilled water for the removal of soluble inorganic ions and then dried at 100 °C for 12 h. Afterwards, the carbon material was ground using mortar and pestle and subsequently sieved through 400-mesh sieve and used for AC synthesis. The carbon yield of $25 \pm 2\%$ was obtained.

Following the pre-carbonization process, the carbon was activated in the activation process using KOH in a 1:1 (w/w basis) ratio by mixing with water (100 mL) in a beaker by constant stirring for a period of 1 h and heated at 100 °C for 36 h. Afterwards, the carbon material was heated in a muffle furnace at 600 °C for a period of 2 h at a heating rate

of 10 °C /min under a limited oxygen atmosphere (Fig. 2). Then, the synthesized activated carbon was cooled down to room temperature and washed with a copious amount of distilled water until the pH of the filtrate was neutral. Afterwards, the activated carbon was filtered and dried in an oven at 100 °C for 12 h, ground, and stored for subsequent use and the activated carbon samples were abbreviated as BFSW-AC.

2.3 Characterization of activated carbon

The surface morphology and pore formation of the carbon obtained from BFSW (before and after activation) were studied by field emission scanning electron microscopy analysis (model: Phenom ProX FESEM). The crystallographic structure of BFSW-AC was identified by X-ray diffraction (XRD) characterization using a Rigaku MiniFlex X-ray diffractometer with Cu K α 1 radiation ($\lambda = 0.15406$ nm). The pore formation on the carbon material after the activation was carried out by surface area analysis at -196 °C using a sorptometer (Quantachrome Instruments, Autosorb IQ series). Prior to analysis, the carbon materials were degassed at 150 °C for 3 h. The surface area and pore size distribution were determined using the Brunauer–Emmett–Teller (BET) and Barrett–Joyner–Halenda (BJH) methods. The zeta potential and the particle size of the carbon material were determined using a Zetasizer (Malvern Instruments Inc., UK). CHN analysis was carried out using a EuroVector CHN analyzer (EA 3000), and the bulk density was found by the ratio of the mass of the dry sample (g) to the volume occupied (mL). The yield of activated carbon was determined by the ratio of the weight of carbon to the weight of the precursor.

2.4 Adsorption experiments

Initially, the batch adsorption tests were carried out using aqueous methylene blue (cationic), rhodamine B (zwitterionic), and reactive red (anionic) dye solutions (100 mL)



Fig. 1 Photographic images of bael fruit and its shell

Table 1 Molecular structure and chemical properties of dyes

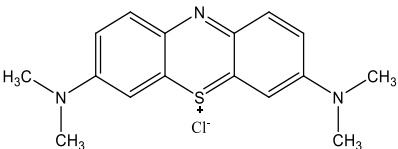
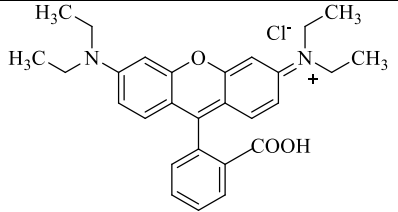
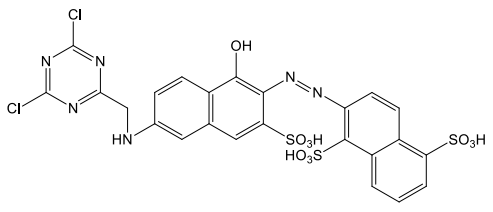
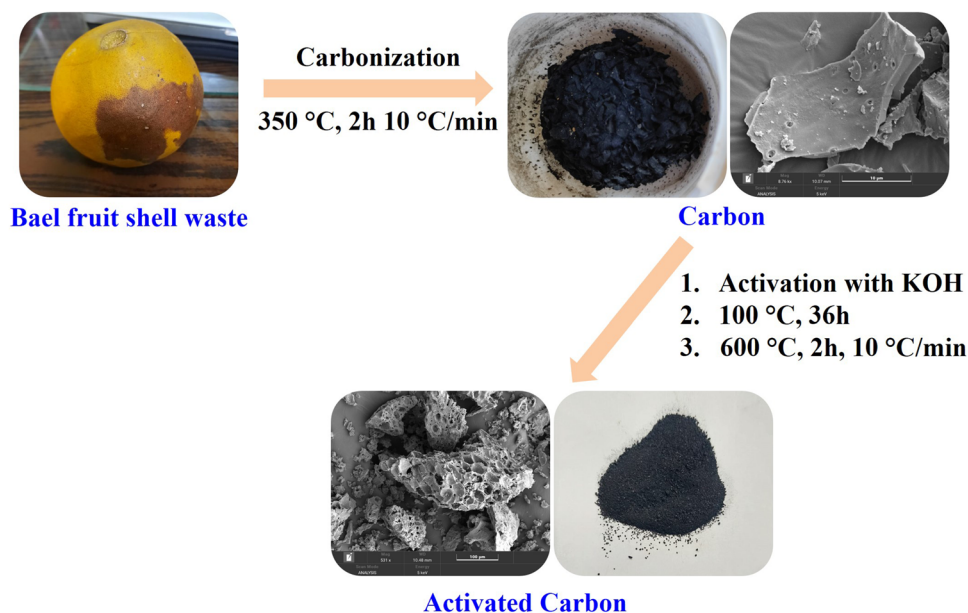
Molecular structure	Chemical Properties	
 <p>Methylene Blue</p>	Chemical formula	C ₁₆ H ₁₈ ClN ₃ S
	Molecular weight	319.85 g/mol
	Absorption maximum	663 nm
	Type	Cationic
 <p>Rhodamine B</p>	Chemical formula	C ₂₈ H ₃₁ ClN ₂ O ₃
	Molecular weight	479.02 g/mol
	Absorption maximum	554 nm
	Type	Zwitterionic
 <p>Reactive red</p>	Chemical formula	C ₂₄ H ₁₆ Cl ₂ N ₆ O ₁₆ S ₃
	Molecular weight	715.52 g/mol
	Absorption maximum	535 nm
	Type	Anionic

Fig. 2 Schematic representation of activated carbon synthesis

separately with activated carbon. Followed by, the varying amounts of adsorbent with 100 mL of aqueous methylene blue dye solution by varying the concentration (100–500 mg adsorbent/100 mL of aqueous dye solution of 10–100 ppm) in a conical flask of 250 mL of glass with stopper were carried out. The mixture was stirred at room temperature using a magnetic stirrer. At predetermined time intervals such as every 15 min for the first 1 h and then every 1 h up to 5 h sampling, and centrifugation (REMI, 12,000 rpm) were performed to separate the activated carbon and the residual dye concentration was determined using a UV–Vis spectrophotometer (Shimadzu UV-2600). The MB dye adsorption reaction was performed in triplicate. Finally, the number of dyes adsorbed (Q_e) per unit mass of activated carbon (BFSW-AC) and the percentage (%) adsorption was calculated using the following equation (Eqs. 1 and 2):

$$Q_e = \{(C_0 - C_t) \times V\} / m \times 1000 \quad (1)$$

$$\text{Percentage adsorption (\%)} = \{C_0 - C_t / C_0\} \times 100 \quad (2)$$

where C_0 is the initial concentration and C_t is the concentration of the dye at time t (ppm), m is the mass of the adsorbent (g), and V is the volume of the solution (L).

2.5 Adsorption isotherms

Adsorption isotherms are important to determine the adsorption potential of the adsorbent and to define the dye-carbon interaction relationship to describe how the adsorbate molecules distribute between solid and liquid phases when the process reaches a state of equilibrium. In order to optimize the design of an adsorption system for the adsorption of MB dye on BFSW-AC, the adsorption data were fitted to Langmuir and Freundlich isotherms to explain the equilibrium state of the adsorption process.

2.5.1 Langmuir isotherm

The Langmuir isotherm was developed to explain how adsorption occurs on a homogenous surface. The linearized form of Langmuir model is as follows:

$$\frac{C_e}{Q_e} = \frac{1}{K_L q_m} + \frac{C_e}{q_m} \quad (3)$$

where q_m is the maximum adsorption capacity (mg/g) and K_L is the Langmuir constant related to the energy for adsorption (L/mg), which is calculated from the slope and intercept of the linear plot (C_e/Q_e Vs C_e).

2.5.2 Freundlich isotherm

The Freundlich isotherm is mainly applied to explain how adsorption occurs on a heterogenous surface. In this study, this model was applied to discuss the MB dye and carbon particle interaction relationship.

$$\ln Q_e = \frac{1}{n} \ln C_e + \ln k_F \quad (4)$$

where Q_e is the amount of dye adsorbed at equilibrium time (mg/g); C_e is the equilibrium concentration of dye in solution (mg/L); k_F is the Freundlich adsorption parameter; and $1/n$ is the heterogeneity factor, which can be calculated from the slope and intercept of the linear plot of $\ln Q_e$ against $\ln C_e$. A value of $n > 1$ denotes a favorable adsorption system.

2.6 Adsorption kinetics

The kinetic modeling of the adsorption process gives out information about the mechanism of adsorption, which is essential for process efficiency. The present study involves the use of kinetic models such as pseudo-first-order and pseudo-second-order models for modeling the kinetics of adsorption of MB dye into BFSW-AC.

2.6.1 Pseudo-first-order kinetics

The pseudo-first-order kinetics model is expressed by

$$\frac{dQ_t}{dt} = k_1 (Q_e - Q_t) \quad (5)$$

While integrating Eq. (5) for the boundary condition at $t=0$ to $t=t$ and $Q=0$ to $Q=Q_t$, the linear form is represented as follows (Eq. 6):

$$\ln(Q_e - Q_t) = \ln Q_e - k_1 t \quad (6)$$

where k_1 is the rate constant of the pseudo-first-order model (min^{-1}), Q_e is the amount of dye adsorbed per unit mass of adsorbent at equilibrium (mg/g), and Q_t is the amount of dye adsorption at time t (mg/g). The rate constant (k_1) of the model can be determined by the slope of the linear plot of $\ln(Q_e - Q_t)$ vs t .

2.6.2 Pseudo-second-order kinetics

The pseudo-second-order kinetics is expressed as follows:

$$\frac{dQ}{dt} = k_2 (Q_e - Q_t)^2 \quad (7)$$

The above equation can be rearranged as follows:

$$\frac{dQ}{(Q_e - Q_t)^2} = k_2 dt \quad (8)$$

While integrating the above equation at $t=0$ to $t=t$ and $Q=0$ to $Q=Q_e$, the equation can be rearranged as below.

$$\frac{1}{(Q_e - Q_t)} = \frac{1}{Q_e} + k_2 t \quad (9)$$

$$\frac{t}{Q_t} = \frac{1}{k_2 Q_e^2} + \frac{t}{Q_e} \quad (10)$$

where k_2 is the rate constant of pseudo-second-order model (g/mg min) and Q_e is the amount of dye adsorption at equilibrium (mg/g). The value of Q_e can be determined from the slope and intercept of linear plot of t/Q_t vs t .

3 Results and discussion

3.1 XRD analysis

The XRD patterns of BFSW-derived carbon before and after activation with KOH are shown in Fig. 3. The diffraction peak at 24.8° and 44.34° are assigned to the reflection from the (002) and (100)/(101) planes of carbon materials, attributed to the graphitic nature of the carbon, and the obtained activated carbon is amorphous in nature [31, 32]. The intensity of these broad peaks is enhanced as a result of KOH activation by heat treatment which showed the enhanced graphitic structure formation [33]. Furthermore, it could be attributed to the presence of potassium compounds in the

carbon materials after activation with KOH [34]. In general, KOH treatment of activated carbon would result in the complete removal of lactone and carboxy groups that would decrease the acidic and basic groups roughly between 8 and 9% [35].

3.2 FE-SEM analysis

The creation of pores in the carbon material by activating the carbon materials with KOH was determined by FE-SEM analysis. The FE-SEM images of BFSW carbon before and after activation are presented in Fig. 4. The results revealed that no pores can be seen in BFSW carbon before activation, and it looks like a uniform thin film with a smooth surface. However, a macro-porous structure with a rough texture can be clearly observed after activation with KOH (BFSW-AC), which was further confirmed by surface area analysis. Similar pore formation was observed by Ozsin et al. [36] in the activation of carbon by KOH obtained from agricultural waste of chickpea.

3.3 Surface area, bulk density, and particle size analysis of BFSW-AC

The pore formation after activation with KOH was confirmed by surface area analysis. BFSW-activated carbon has a higher specific surface area of $944.09 \text{ m}^2/\text{g}$ compared to the carbon obtained before activation, which has a lower specific surface area of $2.43 \text{ m}^2/\text{g}$. The significant enhancement in the surface area obviously indicates pore creation after activation with KOH and validated the FE-SEM results. The N_2 adsorption isotherms of carbon material before and after activation are exhibiting type I isotherm which is usually observed for microporous materials. Furthermore, the

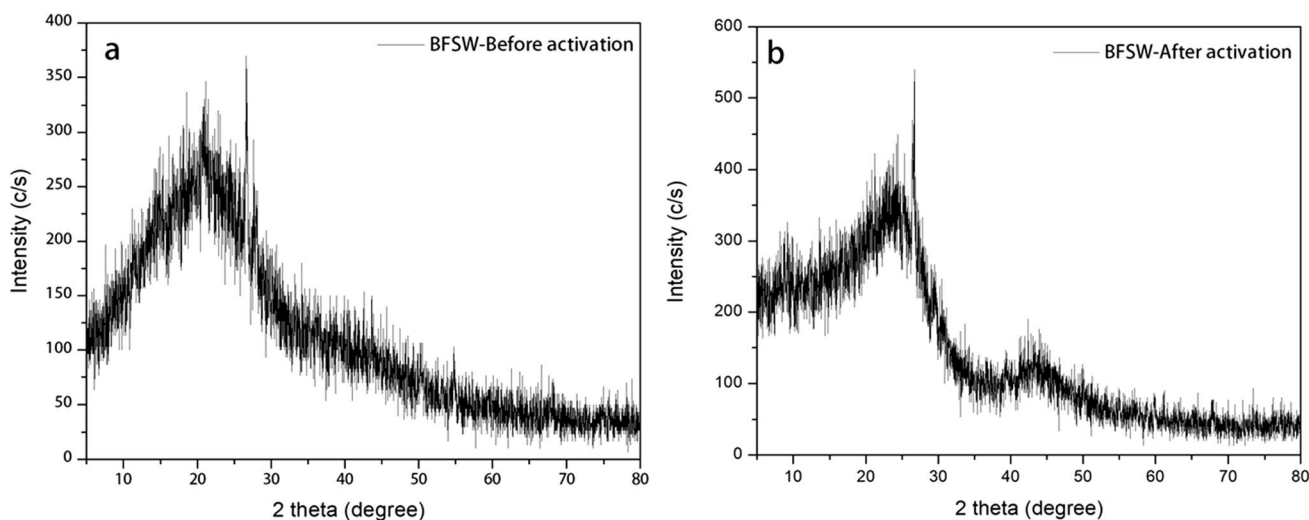


Fig. 3 XRD pattern of BFSW-derived carbon **a** before activation and **b** after activation

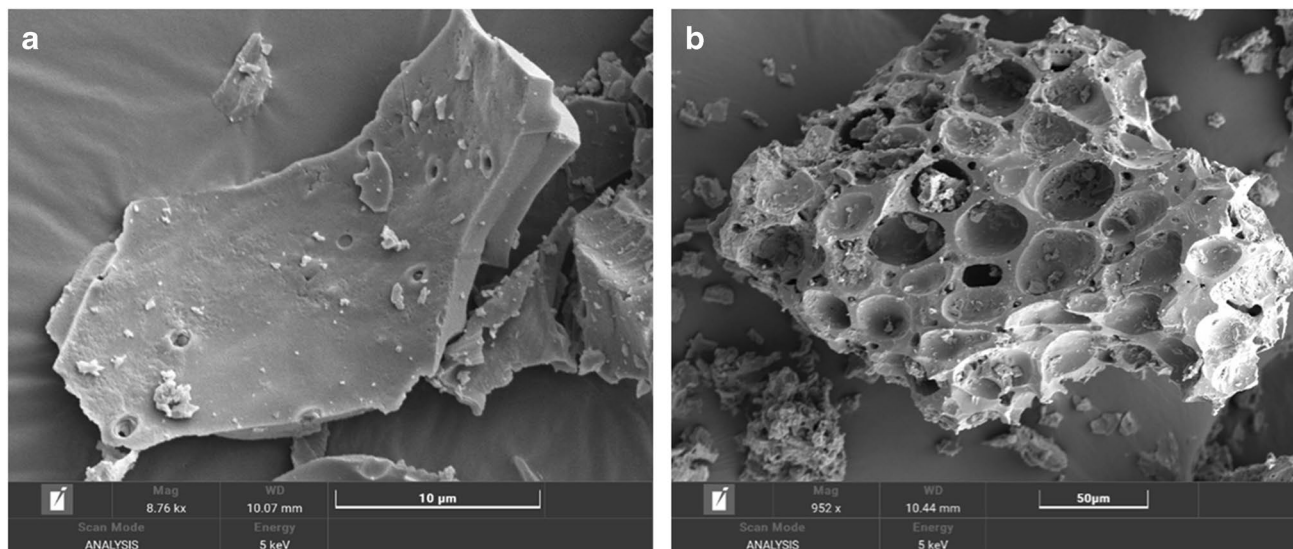


Fig. 4 FE-SEM image of carbon **a** before activation and **b** after activation

bulk density is also an important factor that influences the design of commercial adsorption columns and is inversely proportional to the particle size of the adsorbent. The bulk density was found to be 0.4 g/cm^3 for BFSW-AC, which is beyond the lower limit set by the American Water Works Association at a value of 0.25 g/cm^3 for field application [37]. Furthermore, the average particle size of the synthesized activated carbon material is 282.6 nm.

3.4 CHNS analysis

The CHNS analysis revealed that the BFSW contains 44.368% C, 46.609% O, 7.239% H, and 1.784% N and the carbon percentage is increased to 66.333%, whereas the oxygen, hydrogen, and nitrogen content is decreased to 27.132%, 5.043%, and 1.492% after carbonization. Furthermore, after activation with KOH, the carbon percentage was significantly enhanced to 93.032%, whereas the oxygen and hydrogen decline to 2.531% and 4.437% and the nitrogen content is completely removed. The significant enhancement in the carbon percentage is attributed to the fact that the KOH activation followed by heat treatment intensified the complete decomposition of lignocellulose materials. Similar results were obtained by Thongpat et al. [38] during the preparation of microporous activated carbon from rubberwood by activating with KOH.

3.5 FTIR analysis

From FTIR spectra of carbon before activation, the band at $3151\text{--}3334 \text{ cm}^{-1}$ may be attributed to the stretching band of N–H and O–H due to amine and carboxylic acid groups,

respectively. The peak at $1760\text{--}1612 \text{ cm}^{-1}$ can be attributed to the stretching band of C=O due to the presence of the carboxylic acid group while the peak at 1605 cm^{-1} indicates the presence of N–H bend due to the 1° amine group or stretch vibrations of C=C bonds. The broad sharp peak at $1000\text{--}1404 \text{ cm}^{-1}$ is attributed to the C–C stretching of aromatics and C–N stretching due to aliphatic amines while the absorption peak at 932 cm^{-1} indicates the aromatic C–H bending vibration.

From the FTIR spectra of activated carbon after activation with KOH, changes in the spectrum occurred (Fig. 5).

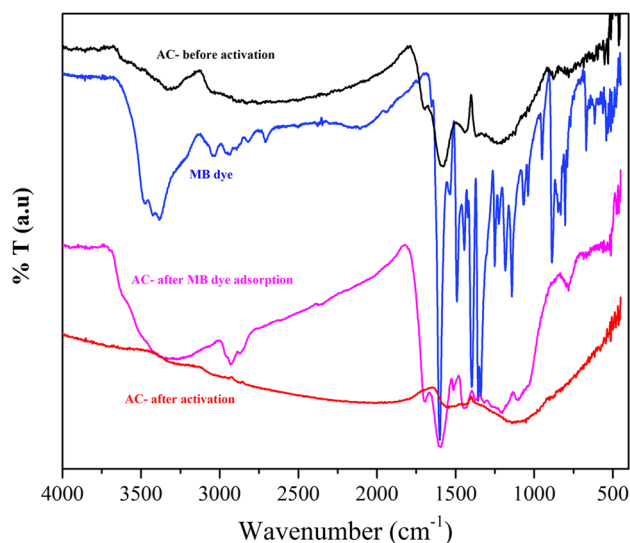


Fig. 5 FTIR spectra of activated carbon (before and after activation), after MB dye adsorption, and MB dye

The wave number at 3334 cm^{-1} is corresponding to the $-\text{OH}$ stretching in hydroxyl functional groups. Similar to carbon before activation, the broad peak at $1760\text{--}1607\text{ cm}^{-1}$ is observed which indicates the stretching band of $\text{C}=\text{O}$ due to carboxylic acids. The adsorption intensity of the $\text{C}-\text{C}$ stretch of the aromatic group at 1404 cm^{-1} decreased after activation of carbon. The broad stretching peak from 1233 to 1134 cm^{-1} belongs to the $\text{C}-\text{O}$ or $\text{C}-\text{O}-\text{C}$ stretching. The absorption intensity of $\text{C}-\text{H}$ bending due to the carboxylic acid group decreased after activation of carbon.

From the FTIR spectra of MB dye, the bands at 3413 cm^{-1} , 1603 cm^{-1} , 1401 cm^{-1} , and 1143 cm^{-1} were observed. The band at 3413 cm^{-1} can be attributed to $-\text{OH}/-\text{NH}$ overlapped stretching vibration whereas the peak at 2963 cm^{-1} indicates the symmetrical stretching $\text{C}-\text{H}$ of the $-\text{CH}_2$ band. The peak at 1603 cm^{-1} can be attributed to the $\text{N}-\text{H}$ bend while the absorption peak at $1493\text{--}1401\text{ cm}^{-1}$ belong to the stretching band of the $\text{C}-\text{C}$ group. The bands at 1251 cm^{-1} and 1143 cm^{-1} belong to the stretching band of $\text{C}-\text{N}$ from the amide group and $\text{C}-\text{O}$ from the carboxylic group, respectively. The strong peak at 888 cm^{-1} indicated the bending band of $\text{C}-\text{H}$ from the aromatic functional group.

The FTIR spectrum of activated carbon after adsorption of MB dye is found to be similar to that of carbon before activation with KOH . There is a strong increase in the band intensity of $\text{N}-\text{H}$ and $\text{O}-\text{H}$ stretching between 3709 and 3000 cm^{-1} due to an increase in the adsorption of MB dye on carbon. The peak of $\text{C}-\text{H}$ of the $-\text{CH}_2$ band of MB dye shifted from 2963 to 2942 cm^{-1} after adsorption in carbon while the peaks at 1706 cm^{-1} and 1613 cm^{-1} indicated the stretching band of $\text{C}=\text{O}$ due to carboxylic acids and $\text{N}-\text{H}$ bend in the carbon and dye, respectively. The absorption peaks at 1493 cm^{-1} , 1251 cm^{-1} , and 1143 cm^{-1} of methylene blue dye disappeared after adsorption of methylene blue dye. The peak appearing at 802 cm^{-1} indicates the adsorption of the aromatic group of MB dye in carbon.

3.6 Adsorption of dye pollutants

3.6.1 Preliminary study on adsorption of MB dye

Initially, the adsorption capacity of a raw bael fruit shell and carbonized and activated carbon materials are investigated, and the results are shown in Fig. 6. The results revealed that 68 and 59% of MB dye got adsorbed on bare bael fruit shell and carbonized materials, whereas it was significantly enhanced to 94.15% using carbon activated with KOH . The enhancement in the adsorption capacity could be attributed to the fact that the volatile matters are thermo-chemically decomposed during the activation stage which creates pores and enhances the surface area of activated carbon. Furthermore, the results

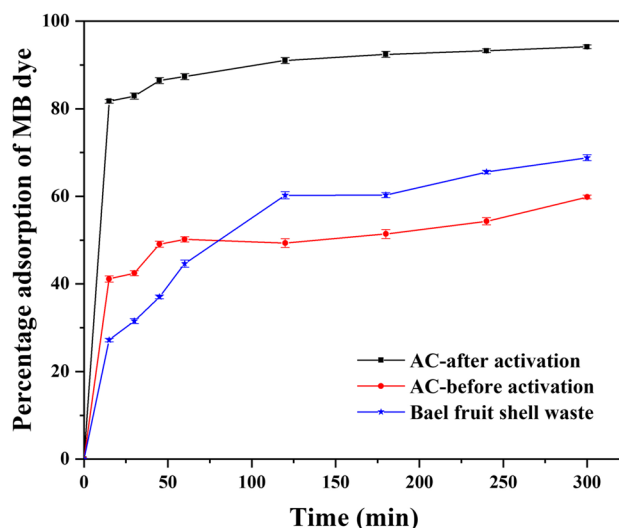


Fig. 6 Percentage adsorption of MB dye using bare bael fruit shell (BFS), carbonized (AC-before activation), and activated carbon (AC-after activation) materials with the standard error value

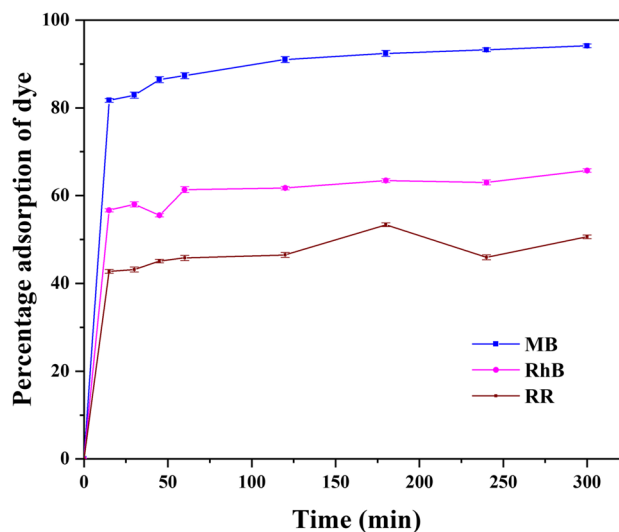


Fig. 7 Effect of dye type on adsorption capacity of BFSW-AC with the standard error value

validate that the activated carbon could be an efficient adsorbent for the removal of methylene blue dye.

3.6.2 Effect of surface charge and type of pollutants on adsorption

Three types of pollutants, namely methylene blue (cationic), rhodamine B (zwitterionic), and reactive red (anionic) dyes, were chosen, and the adsorption reaction was performed with a dye concentration of 50 ppm and 300 mg of activated carbon (Fig. 7). The results demonstrated that the maximum

adsorption of 94.15% was obtained for MB dye compared to the other adsorbates that showed comparatively low percentages of adsorption of 65.71% and 50.59% for RhB and RR dyes, respectively. The zeta potential value reveals the surface charge of the activated carbon. The zeta potential of BFSW-AC was measured to analyze the magnitude of charge attraction/repulsion among the particles to determine the material's suitability. The result revealed that the zeta potential of activated carbon is -16.2 mV. The negative value of zeta potential implies that the net charge of the activated carbon is negative. Therefore, the significant adsorption towards the MB dye is due to the electrostatic attraction between the cationic MB dye and negative surface of activated carbon (Fig. 8). Thus, the negatively charged BFSW-AC is found to be effective in MB dye removal due to the huge availability of a negatively charged surface that enhanced the rate of ionization and protonation of the adsorbent's hydroxyl and oxygen groups [39]. Furthermore, the RhB and RR dye showed some adsorption towards activated carbon, although lower than that of the MB dye. The lower adsorption may be attributed to the presence of a negative charge on the RhB ($-\text{COOH}$, zwitterionic) and RR dye ($-\text{SO}_3\text{H}$, anionic).

Similarly, Lim et al. [40] studied the effect of adsorbent surface charge and type of dyes on the adsorption capacity of $\text{Ti}_3\text{C}_2\text{-MXenes}$. They demonstrated that anionic dyes showed higher adsorption towards negatively charged $\text{Ti}_3\text{C}_2\text{-MXene}$ adsorbent through electrostatic attraction. Therefore, the MB dye has been chosen for all subsequent adsorption studies for optimizing the influence of different reaction operational

parameters on the adsorption capacity of prepared activated carbon.

3.6.3 Effect of adsorbent dosage

The adsorbent concentration is among the major parameters that need to be primarily considered which impart efficient adsorption of dyes. For this study, varying amounts of activated carbon (100, 200, 300, and 500 mg) were experimented at a constant initial dye concentration of 50 ppm at

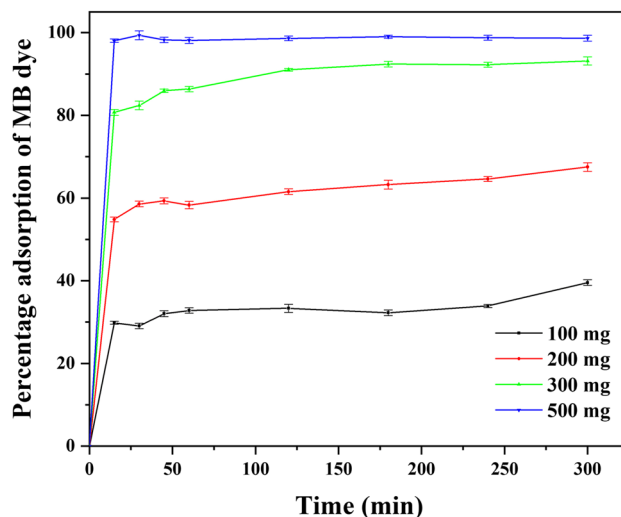


Fig. 9 Effect of activated carbon amount on adsorption of MB dye with the standard error value

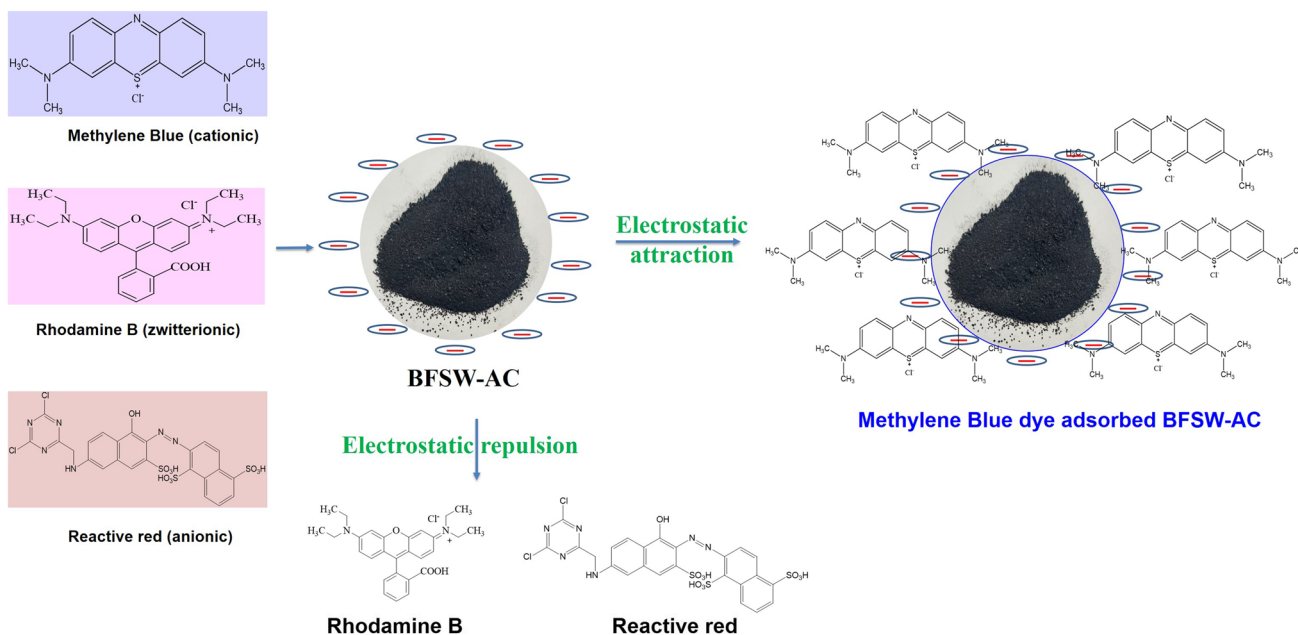


Fig. 8 Schematic representation of adsorption of MB dye on BFSW-AC

different time intervals (15–300 min). Figure 9 shows the plot of the percentage of MB dye adsorbed at varying time intervals at varying adsorbent amounts.

While varying the amount of adsorbent at a fixed MB dye concentration of 50 ppm, it was observed that the initial adsorption of dye increased with an increase in the amount of the adsorbent. It was also observed that the adsorption of dyes with a high amount of activated carbon reached equilibrium earlier than those with a low share of carbon. Thus, the adsorption of MB dye, with the increase in the dose of adsorbent, on the surface of the adsorbent was faster but that ended up with a lower adsorbate concentration in bulk solution than the low adsorbent dose condition. Also, for adsorption of MB dye of 50 ppm, an optimal point for adsorption was attained remarkably rapidly at a time interval of 15 to 45 min, which shows the highly absorptive nature of the carbon. Furthermore, the rapid adsorption of dyes would be advantageous for field applications for effective adsorption of dye-containing effluents. At varying concentrations of the adsorbent, the rate of adsorption was found to be 40.04% (100 mg), 68.0% (200 mg), 94.15% (300 mg), and 99.64% (500 mg). Thus, it was observed that the increase in the adsorbent dosage from 100 to 500 mg results in the decrease of the amount of dye adsorbed (Q_e) from 21.25 to 10.69 mg/g with the increase in the percentage of dye removal from 40.04 to 99.64%. The optimum is considered 300 mg (with a drop in Q_e from 21.25 to 16.83 mg/g), although a higher adsorption rate was attained while using 500 mg of carbon (i.e., Q_e decreased from 21.25 to 10.69 mg/g) considering the rate of increase with regard to the quantity of the adsorbent to arrive at a most economical minimal dosage to benefit large-scale applications. Hence, further studies were continued with varying amount of initial dye concentrations (10–100 ppm) with an adsorbent amount of 300 mg.

3.6.4 Effect of initial MB dye concentration

The initial dye concentration has a significant effect during its adsorption from effluents/aqueous solutions. For this study, the effects of varying initial concentrations of MB dye (10, 25, 50, 75, and 100 ppm) on the adsorptive removal of dye using fixed activated carbon (300 mg) were experimented at different time intervals (15–300 min) as shown in Fig. 10.

It was found that the percentage of dye adsorbed decreased with increasing initial concentration of MB dye from 25 to 100 ppm. The initial dye concentration gives a driving force against the resistance to the mass transfer of dye and adsorbent, i.e., between the aqueous solution and the solid phase of the adsorbent. At the same time, the percentage of dye removal decreased from 99.75% (25 ppm)

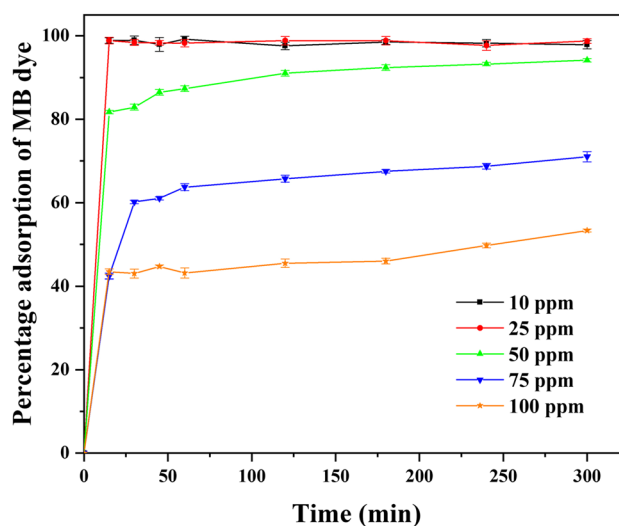


Fig. 10 Effect of initial MB dye concentration on adsorption efficiency with the standard error value

to 52.80% (100 ppm) with the increase in the initial MB dye concentration from 25 to 100 ppm. However, there is no prominent difference in the % of adsorption between 10 ppm (98.86%) and 25 ppm (99.75%). Thus, the high concentration of initial dye led to the accumulation of dye molecules on the adsorbent surface, which causes the saturation of active sites on the adsorbent surface, therein decreasing the percentage of dye removal. Furthermore, the amount of adsorption increases within the time interval of 15 to 45 min and then slowed down with a further increase in the contact time, which reveals the highly adsorptive nature of the activated carbon produced. It is observed that there is an increase in the amount of dye adsorbed from 2.84 to 16.82 mg/g at an increasing initial dye concentration ranging between 10 and 50 ppm. However, beyond this, there is a slight drop in the amount of dye adsorbed from 16.82 mg/g at 50 ppm to 16.28 mg/g and 15.67 mg/g at an initial dye concentration of 75 ppm and 100 ppm, respectively. So, an adsorbent dose of 300 mg for an initial MB dye concentration of 50 ppm was found to be optimal for a higher percentage of adsorption. Although the percentage of adsorption, i.e., 94.15%, at 50 ppm is lower than the removal attained at 25 ppm, i.e., 99.75%, still it is found to be an optimal concentration considering the commercial application.

3.6.5 Effect of initial solution pH

The initial pH of the aqueous solution influences the adsorption process by affecting the surface of the adsorbent and the chemistry of the adsorbate [41]. Figure 11 shows the percentage of adsorption against varying time intervals with different initial pH values of the dye solution.

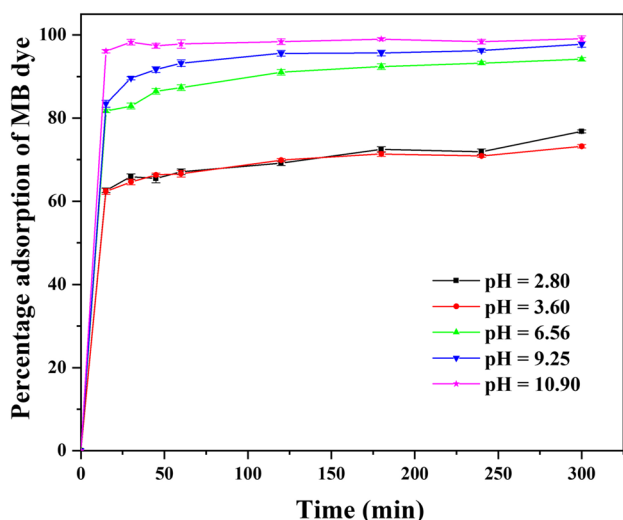


Fig. 11 Effect of initial pH of dye solution on adsorption of MB dye with the standard error value

The percentage of adsorption was found to be 77.30%, 73.21%, 94.15%, 97.26%, and 99.60% at a solution pH of 2.80, 3.60, 6.56, 9.25, and 10.9, respectively. Thus, there is an increase in the amount of MB dye adsorbed with the increase of the solution pH. So, when the pH increased, the H^+ ions in the solution decreased. This results in less competition between dye molecules and positive ions, thereby ending up with a greater number of negatively charged sites by means of oxygenated group dissociation and formation of MB-oxygen binding sites that favor cationic dye adsorption. Hence, MB dye revealed excellent adsorption in a basic medium because of its cationic properties. In contrast, in an acidic medium, the adsorbent becomes more positively charged, and hence, the number of positively charged sites increases, which hinder the dye adsorption due to electrostatic repulsion. A similar behavior for MB dye adsorption was reported on biomass-based carbon [41–43].

3.7 Adsorption isotherms

Adsorption isotherms aid to understand the relationship between the adsorbate and the adsorbent at a given temperature. Langmuir and Freundlich isotherms are applied, and the results are elucidated in Fig. 12. The Langmuir isotherm model is suitable for monolayer adsorption of dye on the adsorbent as a finite number of identical sites whereas the Freundlich isotherm is suited for multilayer adsorption on the adsorbent surface with an assumption of heterogenous surface by means of non-uniform distribution of adsorbed molecules over the adsorbent surface [44]. Here, the adsorption of MB dye on the BFSW-AC adsorbent agrees with the Langmuir isotherm with the best fit (R^2 value = 0.9995) than the Freundlich isotherm that exhibited comparatively lower linear regression coefficient determination of 0.7821 (R^2 value).

The maximum adsorption capacity, Q_{max} , of 15.77 mg/g was observed with the Langmuir isotherm, which is higher than those from the existing studies on the removal of MB dye using the carbon synthesized from wheat straw (Q_{max} of 12.03 mg/g), nut shell (Q_{max} of 5.3 mg/g), and fruit wastes (Q_{max} of 10.6 mg/g) [45–47]. Similar experimental finding was also observed by Roy et al. [28] with the best fit with the Freundlich isotherm plot of carbon from BFSW for the adsorptive removal of patent blue dye. This can also be visualized from the experimental and calculated Langmuir isotherm plots of C_e vs Q_e . Thus, the Langmuir adsorption isotherm model showed the best fit for the system of BFSW-AC for MB dye adsorption in terms of maximum linear regression coefficient and the curve fit.

3.8 Adsorption kinetics studies

The pseudo-first-order and pseudo-second-order models are used to analyze the experimental data obtained in order to assess the adsorption kinetics of MB dye on BFSW-AC. The results of the calculated rate constant for different initial dye

Fig. 12 a Langmuir and b Freundlich isotherm models for MB dye adsorption on BFSW-AC.

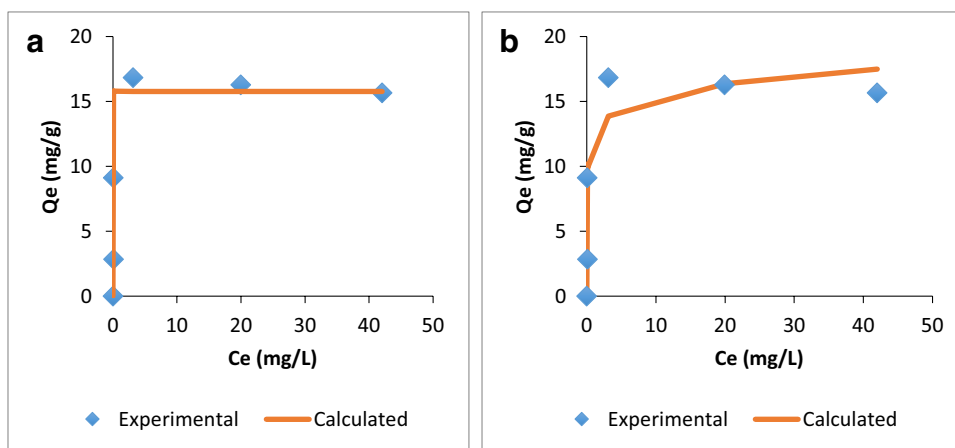
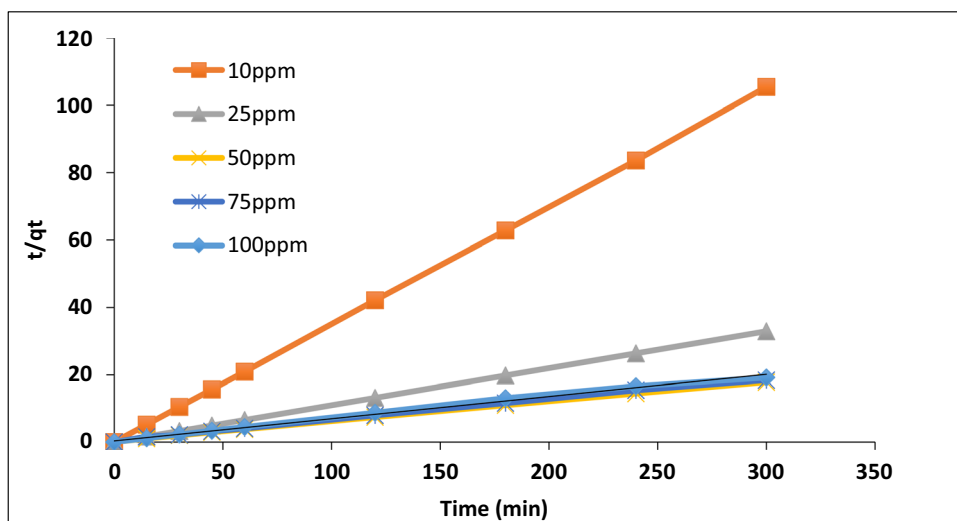


Table 2 Kinetic results of pseudo-first-order and pseudo-second-order models for varying concentrations of MB dye adsorption on BFSW-AC

Initial concentration (mg/L)	Q_e , exp (mg/g)	First-order kinetic model			Second-order kinetic model				
		k_1 (h^{-1})	Q_e , cal (mg/g)	R^2	SSE (%)	k_2 (g/mg h)	Q_e , cal (mg/g)	R^2	SSE (%)
10	2.84	0.004	0.01	0.3161	2.837	1.540	2.85	0.9999	0.009
25	9.11	0.003	0.00	0.9176	9.103	1.698	9.11	1	0.001
50	16.83	0.006	3.73	0.4816	13.095	0.017	16.89	0.9997	0.064
75	16.28	0.006	14.98	0.6616	1.299	0.009	16.31	0.9986	0.035
100	15.67	0.003	10.35	0.9471	5.322	0.011	15.22	0.9945	0.452

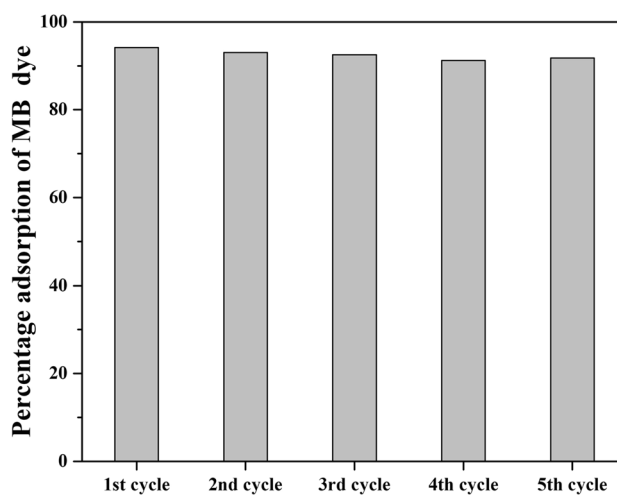
Fig. 13 Pseudo-second-order plot of t/q_t vs time for MB dye adsorption on BFSW-AC

concentrations using pseudo-first-order and pseudo-second-order models are presented in Table 2 and Fig. 13.

For the adsorption process, highest correlation coefficients close to unity ($R^2 = 0.99-1$) were observed for the pseudo-second-order kinetic model against the pseudo-first-order model ($R^2 = 0.31-0.92$). This reveals the soundness of the pseudo-second-order model for MB dye adsorption while using BFSW-activated carbon.

Similarly, several authors observed the best fit with the pseudo-second-order kinetic model for adsorption of MB dye [2, 5, 43]. The results were further demonstrated with the slight deviation between the calculated Q_e against experimental Q_e values for the pseudo-second-order kinetic model (observed from SSE %). This remark supports the assumption that the adsorption occurred primarily by chemisorption [41].

In addition, the regeneration and reusability of adsorbent material is highly essential for commercial scale application. Therefore, after every cycle of the experiment, BFSW-AC was separated by centrifugation and washed with water and dried in an oven for its reusability. The adsorption reaction was repeated up to 5 cycles of experiment and the results revealed that the adsorption capacity of BFSW-AC was retained (Fig. 14).

**Fig. 14** Cyclic run in the adsorption of MB dye using BFSW-AC

4 Conclusion

Activated carbon was successfully synthesized from bael fruit shell waste through carbonization followed by activation using a KOH agent and characterized by various physicochemical techniques. The significant enhancement

in the surface area after activation confirmed the creation of pores on the activated carbon's surface, which was further validated by FE-SEM analysis. Zeta potential analysis revealed the negative surface of the activated carbon. The adsorption results revealed that 300 mg of activated carbon, 50 ppm, and pH 6.56 are the optimum conditions for higher adsorption capacity of activated carbon towards methylene blue pollutant. The adsorption experimental data was best fitted into the Langmuir isotherm and second-order kinetic model ($R^2 = 0.99–1.00$). The mechanism of enhanced adsorption towards MB dye is the electrostatic interaction between the cationic MB dye and negatively charged BFSW-AC surface. The activated carbon material was reused and retained its efficiency up to 5 cycles of adsorption experiment. Herein, it is concluded that synthesizing of activated carbon from waste biomass could be an alternative way to develop an adsorbent for environmental pollutants removal from wastewater.

Acknowledgements The authors thank the director of CSIR-CLRI for the continuous support.

Author contribution VM: Conceptualization, methodology, data curation, writing—original draft preparation, review and editing.

TSN: Conceptualization, methodology, data curation, writing—original draft preparation, review and editing.

Funding CSIR-CLRI Communication No.: 1695. The authors acknowledge the institute for financial support through MLP projects (MLP-19 and MLP-27).

Declarations

Conflict of interest The authors declare no competing interests.

References

- Adegoke KA, Bello OS (2015) Dye sequestration using agricultural wastes as adsorbents. *Water Resour Ind* 12:8–24. <https://doi.org/10.1016/j.wri.2015.09.002>
- Bordoloi N, Dey MD, Mukhopadhyay R, Katak R (2018) Adsorption of methylene blue and rhodamine B by using biochar derived from *Pongamia glabra* seed cover. *Water Sci Technol* 77(3):638–646. <https://doi.org/10.2166/wst.2017.579>
- Dutta S, Gupta B, Srivastava, S.K., & Gupta, A. K. (2021) Recent advances on the removal of dyes from wastewater using various adsorbents: a critical review. *Mater Adv* 2:4497–4531. <https://doi.org/10.1039/d1ma00354b>
- Yagub MT, Sen TK, Afroz S, Ang HM (2014) Dye and its removal from aqueous solution by adsorption: a review. *Adv Colloid Interface Sci* 209:172–184
- Hameed BH, Ahmad AA (2009) Batch adsorption of methylene blue from aqueous solution by garlic peel, an agricultural waste biomass. *J Hazard Mater* 164(2–3):870–875. <https://doi.org/10.1016/j.jhazmat.2008.08.084>
- Lellis B, Fávoro-Polonio CZ, Pamphile JA, Polonio JC (2019) Effects of textile dyes on health and the environment and bioremediation potential of living organisms. *Biotechnol Res Innov* 3(2):275–290. <https://doi.org/10.1016/j.biori.2019.09.001>
- Aragaw TA, Bogale FM (2021) Biomass-based adsorbents for removal of dyes from wastewater: a review. *Front. Environ. Sci.* 9:764958. <https://doi.org/10.3389/fenvs.2021.764958>
- Allen SJ, Koumanova B (2005) Decolourisation of water/wastewater using adsorption. *J Univ Chem Technol Metall* 40:175–192
- El-Bery HM, Saleh M, El-Gendy RA, Saleh MR, Thabet SM (2022) High adsorption capacity of phenol and methylene blue using activated carbon derived from lignocellulosic agriculture wastes. *Sci Rep* 12:5499. <https://doi.org/10.1038/s41598-022-09475-4>
- Mousavi SA, Mahmoudi A, Amiri S, Darvishi P, Noori E (2022) Methylene blue removal using grape leaves waste: optimization and modeling. *Appl Water Sci* 12:112. <https://doi.org/10.1007/s13201-022-01648-w>
- Koilraj P, Kannan S (2010) Phosphate uptake behavior of ZnAlZr ternary layered double hydroxides through surface precipitation. *J Colloid Interface Sci* 341:289–297. <https://doi.org/10.1016/j.jcis.2009.09.059>
- Rafatullah M, Sulaiman O, Hashim R, Ahmad A (2010) Adsorption of methylene blue on low-cost adsorbents: a review. *J Hazard Mater* 177:70–80. <https://doi.org/10.1016/j.jhazmat.2009.12.047>
- Efome JE, Rana D, Matsuura T, Lan CQ (2018) Experiment and modeling for flux and permeate concentration of heavy metal ion in adsorptive membrane filtration using a metal-organic framework incorporated nanofibrous membrane. *Chem Eng J* 352:737–744. <https://doi.org/10.1016/j.cej.2018.07.077>
- Efome JE, Rana D, Matsuura T, Lan CQ (2018) Metal-organic frameworks supported on nanofibers to remove heavy metals. *J Mater Chem* 6(10):4550–4555. <https://doi.org/10.1039/C7TA10428F>
- Efome JE, Rana D, Matsuura T, Lan CQ (2018) Insight studies on metal-organic framework nanofibrous membrane adsorption and activation for heavy metal ions removal from aqueous solution. *ACS Appl Mater Interfaces* 10(22):18619–18629. <https://doi.org/10.1021/acsami.8b01454>
- Efome JE, Rana D, Matsuura T, Lan CQ (2019) Effects of operating parameters and coexisting ions on the efficiency of heavy metal ions removal by nano-fibrous metal-organic framework membrane filtration process. *Sci Total Environ* 674:355–362. <https://doi.org/10.1016/j.scitotenv.2019.04.187>
- Park SJ, Kim KD (1999) Adsorption behaviors of CO₂ and NH₃ on chemically surface-treated activated carbons. *J Colloid Interface Sci* 212:186–189. <https://doi.org/10.1006/jcis.1998.6058>
- Deng H, Lu J, Li G, Zhang G, Wang X (2011) Adsorption of methylene blue on adsorbent materials produced from cotton stalk. *Chem Eng J* 172:326–334. <https://doi.org/10.1016/j.cej.2011.06.013>
- El-Nemr MA, Abdelmonem NM, Ismail IMA, Ragab S, El-Nemr A (2020) Removal of Acid Yellow 11 dye using a novel modified biochar derived from watermelon peels. *Dwt* 203:403–431. <https://doi.org/10.5004/dwt.2020.26207>
- Januário EFD, Vidovix TB, Araújo LAd, Bergamasco Beltran L, Bergamasco R, Vieira AMS (2021) Investigation of Citrus reticulata peels as an efficient and low-cost adsorbent for the removal of safranin orange dye. *Environ Tech* 1:1–15. <https://doi.org/10.1080/09593330.2021.1946601>
- Shakir K, Elkafrawy AF, Ghoneimy HF, Beheir SGE, Refaat M (2010) Removal of rhodamine B (a basic dye) and thoron (an acidic dye) from dilute aqueous solutions and wastewater simulants by ion flotation. *Water Res* 44(5):1449–1461
- Thang NH, Khang DS, Hai TD, Nga DT, Tuan PD (2021) Methylene blue adsorption mechanism of activated carbon

- synthesised from cashew nut shells. *RSC Adv* 11:26563–26570. <https://doi.org/10.1039/d1ra04672a>
23. Al-Gheethi AA, Azhar QM, Senthilkumar P, Yusuf AA, Al-Buriah AK, Mohamed RMSR, Al-shaibani MM (2022) Sustainable approaches for removing rhodamine B dye using agricultural waste adsorbents: a review. *Chemosphere* 287:132080. <https://doi.org/10.1016/j.chemosphere.2021.132080>
 24. Malhotra M, Suresh S, Garg A (2018) Tea waste derived activated carbon for the adsorption of sodium diclofenac from wastewater: adsorbent characteristics, adsorption isotherms, kinetics, and thermodynamics. *Environ Sci Pollut Res* 25:32210–32220. <https://doi.org/10.1007/s11356-018-3148-y>
 25. Hou J, Liu Y, Wen S, Li W, Liao R, Wang L (2020) Sorghum-waste-derived high-surface area KOH-activated porous carbon for highly efficient methylene blue and Pb(II) removal. *ACS Omega* 5(23):13548–13556. <https://doi.org/10.1021/acsomega.9b04452>
 26. Baliga MS, Mane PP, Joseph N, Jimmy R (2013) Review on the protective effects of the indigenous Indian medicinal plant, bael (*Aegle marmelos* Correa), in gastrointestinal disorders. *Bioact Food Diet Intervent Liver Gastrointest Dis* :313–324. <https://doi.org/10.1016/b978-0-12-397154-8.00036-1>
 27. Ramakrishna YG, Savithri K, Kist M, Devaraj SN (2015) *Aegle marmelos* fruit extract attenuates *Helicobacter pylori* Llpopolysaccharide induced oxidative stress in Sprague Dawley rats. *BMC Complement Alternat Med* 15(1). <https://doi.org/10.1186/s12906-015-0915-x>
 28. Roy K, Verma KM, Vikrant K, Goswami M, Sonwani RK, Rai BN, Vellingiri K, Kim KH, Giri BS, Singh RS (2018) Removal of patent blue (V) dye using Indian bael shell biochar: characterization application and kinetic studies. *Sustain* 10(8). <https://doi.org/10.3390/su10082669>
 29. Belhachemi M (2021) Chapter 14 - Adsorption of organic compounds on activated carbons, Editor(s): Avelino Núñez-Delgado, Sorbents materials for controlling environmental pollution, Elsevier, p 355–385. <https://doi.org/10.1016/B978-0-12-820042-1.00006-7>
 30. Bhattacharyya KG, SenGupta S, Sarma GK (2014) Interactions of the dye, rhodamine B with kaolinite and montmorillonite in water. *Appl Clay Sci* 99:7–17. <https://doi.org/10.1016/j.clay.2014.07.012>
 31. Kishibayev KK, Serafin J, Tokpayev RR, Khavaza TN, Atchabarova AA, Abduakhytova DA, Ibraimov ZT, Sreńscek-Nazzal J (2021) *J Environ Chem Eng* 9:106798. <https://doi.org/10.1016/j.jece.2021.106798>
 32. Khosrowshahi MS, Mashhadimoslem H, Emrooz HBM, Ghaemi A, Hosseini MS (2022) Green self-activating synthesis system for porous carbons: celery biomass wastes as a typical case for CO₂ uptake with kinetic, equilibrium and thermodynamic studies. 109204. <https://doi.org/10.1016/j.diamond.2022.109204>
 33. Demir M, Kahveci Z, Aksoy B, Palapati NKR, Subramanian A, Cullinan HT, El-Kaderi HM, Harris CT, Gupta RB (2015) Graphitic biocarbon from metal-catalyzed hydrothermal carbonization of lignin. *Ind Eng Chem Res* 54(43):10731–10739. <https://doi.org/10.1021/acs.iecr.5b02614>
 34. Nizam NUM, Hanafiah MM, Mahmoudi E, Halim AA, Mohammad AW (2021) The removal of anionic and cationic dyes from an aqueous solution using biomass-based activated carbon. *Sci Rep* 11:8623. <https://doi.org/10.1038/s41598-021-88084-z>
 35. Lendzion-Bieluń Z, Czekajło Ł, Sibera D, Moszyński D, Sreńscek-Nazzal J, Morawski AW, Wrobel RJ, Michalkiewicz B, Arabczyk W, Narkiewicz U (2017) Surface characteristics of KOH-treated commercial carbons applied for CO₂ adsorption. *Adsorpt Sci Technol* 36(1–2):478–492. <https://doi.org/10.1177/0263617417704527>
 36. Özsin G, Kılıç M, Apaydın-Varol E, Pütün AE (2019) Chemically activated carbon production from agricultural waste of chickpea and its application for heavy metal adsorption: equilibrium, kinetic, and thermodynamic studies. *Appl Water Sci* 9:56. <https://doi.org/10.1007/s13201-019-0942-8>
 37. Ravichandran P, Sugumaran P, Seshadri S, Basta AH (2018) Optimizing the route for production of activated carbon from *Casuarina equisetifolia* fruit waste. *Royal Society Open Science* 5(7):171578. <https://doi.org/10.1098/rsos.171578>
 38. Thongpat W, Taweekun J, Maliwan K (2021) Synthesis and characterization of microporous activated carbon from rubberwood by chemical activation with KOH. *Carbon Lett* 31:1079–1088. <https://doi.org/10.1007/s42823-020-00224-z>
 39. Zhang L, Zhang H, Tian Y, Chen Z, Han Lu (2012) Adsorption of methylene blue from aqueous solutions onto sintering process red mud. *Desalin Water Treat* 47(1–3):31–41. <https://doi.org/10.1080/19443994.2012.696412>
 40. Lim S, Kim JH, Park H, Kwak C, Yang J, Kim J, Ryu SY, Lee J (2021) Role of electrostatic interactions in the adsorption of dye molecules by Ti₃C₂-MXenes. *RSC Adv* 11:6201–6211. <https://doi.org/10.1039/D0RA10876F>
 41. Dawood S, Sen TK, Phan C (2016) Adsorption removal of methylene blue (MB) dye from aqueous solution by bio-char prepared from *Eucalyptus sheathiana* bark: kinetic, equilibrium, mechanism, thermodynamic and process design. *Desalin Water Treat* 57(59):28964–28980. <https://doi.org/10.1080/19443994.2016.1188732>
 42. Al-Ghouthi MA, Al-Absi RS (2020) Mechanistic understanding of the adsorption and thermodynamic aspects of cationic methylene blue dye onto cellulosic olive stones biomass from wastewater. *Sci Rep* 10:15928. <https://doi.org/10.1038/s41598-020-72996-3>
 43. Natarajan TS, Bajaj HC, Tayade RJ (2014) Preferential adsorption behavior of methylene blue dye onto surface hydroxyl group enriched TiO₂ nanotube and its photocatalytic regeneration. *J Colloid Interface Sci* 433:104–114. <https://doi.org/10.1016/j.jcis.2014.07.019>
 44. Kalam S, Abu-Khamsin SA, Kamal MS, Patil S (2021) Surfactant adsorption isotherms: a review. *ACS Omega* 6(48):32342–32348. <https://doi.org/10.1021/acsomega.1c04661>
 45. Ragupathy S, Raghu K, Prabu P (2015) Synthesis and characterization of TiO₂ loaded cashew nut shell activated carbon and photocatalytic activity on BG and MB dyes under sunlight radiation. *Spectrochim. Acta Part A Mol Biomol Spectrosc* 138:314–320
 46. Liu Y, Zhao X, Li J, Ma D, Han R (2012) Characterization of bio-char from pyrolysis of wheat straw and its evaluation on methylene blue adsorption. *Desalin Water Treat* 46:115–123
 47. Aboua KN, Yobouet YA, Yao KB, Goné DL, Trokourey A (2015) Investigation of dye adsorption onto activated carbon from the shells of Macoré fruit. *J Environ Manag* 156:10–14

Publisher's note Springer Nature remains neutral with regard to jurisdictional claims in published maps and institutional affiliations.

Springer Nature or its licensor holds exclusive rights to this article under a publishing agreement with the author(s) or other rightsholder(s); author self-archiving of the accepted manuscript version of this article is solely governed by the terms of such publishing agreement and applicable law.